Synthesis and Characterization of Poly(fluorene)-Based Copolymers Containing Various 1,3,4-Oxadiazole Pendants

HSIAO-HSIEN SUNG, HONG-CHEU LIN

Department of Materials Science and Engineering, National Chiao Tung University, Hsinchu, Taiwan, ROC

Received 1 November 2004; accepted 13 January 2005
DOI: 10.1002/pola.20741
Published online in Wiley InterScience (www.interscience.wiley.com).

ABSTRACT: A series of soluble alternating poly(fluorene)-based copolymers containing electron-transporting 1,3,4-oxadiazole (OXD) and hole-transporting carbazole pendants attached to the C-9 position of fluorene units by long alkyl spacers were synthesized. These copolymers possess mesogenic and nonmesogenic pendants attached to a rigid mesogenic poly(fluorene) (PF) backbone. All these polymers exhibit glass-forming liquid crystalline properties, including the nematic and smectic A (SmA) phases, and reveal much wider mesophasic temperature ranges than that of PF. The thermal properties and mesomorphism of these conjugated polymers are mainly affected by the nature of these pendants, and thus the mesophasic temperature ranges and glass-forming properties are greatly enhanced by introducing the OXD pendants. In addition, the tendencies of crystallization and aggregation of PF are also suppressed by introducing the OXD pendants. A single layer device with P4 as an emitter shows a turn-on voltage of 5 V and a bright luminescence of 2694 cd/m^2 at 11 V with a power efficiency of 1.28 cd/A at 100 mA/cm^2. © 2005 Wiley Periodicals, Inc. J Polym Sci Part A: Polym Chem 43: 2700–2711, 2005
Keywords: carbazole; glass-forming property; mesomorphism; oxadiazole (OXD) pendant; poly(fluorene)

INTRODUCTION

Poly(fluorene) (PF) is a well-known high mobility hole transporting blue-emitting polymer for practical applications in polymer light-emitting diodes (PLEDs).[1,2] This material displays extremely high photoluminescence (PL) efficiencies in both solution and solid states.[3,4] However, PF has two major deficiencies as a potential candidate for blue PLEDs. First, PF tends to aggregate and form excimers on heating during device formation or operation under forward biases, therefore, leading to blue-green emission and fluorescence quenching.[5,6] Second, there is an unbalance in charge injection and transportation due to large injection barriers and different charge carrier mobilities.[7] To overcome these drawbacks, the physicochemical properties of PF are improved via side-chain substitution at the C-9 position of the fluorene units. When bulky groups are incorporated into the C-9 position of the fluorene units, it can not only provide large steric hindrance and reduce interchain interaction but also enhance good thermal and morphological stability without substantially changing the electronic properties of the polymer backbone.[8,9] In addition, the introduction of electron-deficient OXD groups into the C-9 position of the fluorene units will increase the electron affinity of resulting polymers and lead to a more

Correspondence to: H.-C. Lin (E-mail: linhc@cc.nctu.edu.tw)

Journal of Polymer Science: Part A: Polymer Chemistry, Vol. 43, 2700–2711 (2005)

balanced charge injection and transportation as well as recombination.[10,11]

Linearly polarized blue organic light-emitting diodes have been demonstrated by taking advantage of the thermotropic mesomorphism to be aligned on a rubbing polyimide (PI) substrate.[12–14] These liquid crystalline materials possess a potential for spontaneous uniaxial alignment of nematic mesomorphism by spin-coating on a rubbing substrate and, therefore, they are enabled to generate polarized light emission. PF and monodisperse oligofluorenes are among the most promising candidates for efficient polarized blue luminescence.[15–21] One of the best devices with monodisperse oligofluorenes as an emitter displays polarized electroluminescence (EL) and the dichroic ratio is as high as 31.[22] It also was found that the side-chain length, pendant structure, and molecular aspect ratio affect the solid morphology, thermotropic properties, and phase transition temperatures of the resulting polymers. Moreover, the absorption and photoluminescence dichroic ratios are influenced as well.[23,24]

Herein, we synthesize the first series of PF with electron-transporting mesogenic pendants in the C-9 position of the fluorene units by long alkyl spacers. This design is based on the consideration that the mesogenic groups with electron-transporting capacity are introduced as pendants to the hole-transporting PF backbones. We hope these functionalized polymers can take advantage of introducing bulky mesogenic pendants to avoid the tendency of spontaneous aggregation and crystallization normally encountered with PF, and to enhance the charge carrier balance as well as the mesophasic temperature range. On the other hand, we also introduce nonmesogenic groups to the PF backbones as pendants for comparative purposes. These intrinsic features help us to investigate the effect of mesogenic pendants on electronic, photonic, and thermotropic properties of the resulting polymers.

EXPERIMENTAL

Measurements

^{1}H NMR spectra were recorded on a Varian unity 300*M* Hz spectrometer using $CDCl_3$ solvent. Elemental analyses were performed on a HERAEUS CHN-OS RAPID elemental analyzer. Transition temperatures were determined by differential scanning calorimetry (Perkin–Elmer Diamond) with a heating and cooling rate of 10 °C/min. The mesophases were studied using a polarizing optical microscope (Leica DMLP) equipped with a hot stage. Thermogravimetric analysis (TGA) was conducted on a Du Pont Thermal Analyst 2100 system with a TGA 2950 thermogravimetric analyzer under a heating rate of 20 °C/min. Gel permeation chromatography (GPC) analysis was conducted on a Water 1515 separation module using polystyrene as a standard and THF as an eluant. UV-visible absorption spectra were recorded in dilute chloroform solutions (10^{-5} M) on a HP G1103A spectrophotometer, and fluorescence spectra were obtained on a Hitachi F-4500 spectrophotometer. Polymer thin films were spin-coated on a quartz substrate from chloroform solutions with a concentration of 10 mg/mL (this condition consists with that of the electroluminescent device). Fluorescence quantum yields were determined by comparing the integrated PL density of a reference 9,10-diphenylanthracene in toluene with a known quantum yield (ca. 5×10^{-6} M, quantum yield = 1.0). Cyclic voltammetry (CV) was performed at a scanning rate of 100 mV/s on a BAS 100 B/W electrochemical analyzer, which was equipped with a three-electrode cell. Pt wire was used as a counter electrode, and Ag/AgCl was used as a reference electrode in the CV measurement. The polymer thin film was cast onto a Pt disc as a working electrode with ferrocene as a standard in acetonitrile, and 0.1 M tetrabutylammonium hexafluorophosphate ($TBAPF_6$) was used as a supporting electrolyte. A series of double-layer EL devices with the configuration of ITO/PEDOT:PSS/Polymer/Ca/Al were made by spin-coating the polymer solutions (with a concentration of 10 mg/mL) onto PEDOT coated glass substrates. The thicknesses of these films were measured on a Sloan DektakIIA surface profilometer. The thickness of PEDOT was about 40 nm, and the thicknesses of these polymers for P1 and P2-P4 were about 60 nm and 80 nm, respectively. The luminance-current-voltage characteristics were recorded on a power source (Keithley 2400) and photometer (MINOLTA CS-100A). To align the LC state into a monodomain, polymers were spin-coated from a 1 wt % solution in chloroform at 2500 rpm onto a glass substrate coated with a polyimide alignment layer. After vacuum-drying, pristine films were thermally annealed at corresponding mesomophic temperature ranges for 30–60 min, then cooled to room temperature.

Materials

Chemicals and solvents were reagent grades and purchased from Aldrich, ARCROS, TCI, and Lancaster Chemical Co. Dichloromathane and THF were distilled to keep anhydrous before use. The other chemicals were used without further purification. Compounds 2-7 and fluorine derivative monomer were synthesized by modified procedures (shown in Scheme 1) that have been described in refs 25–30.

M1

2.25 g (4.77 mmol) of 7a was added to a solution of 2,7-dibromofluorene (0.72 g, 2.22 mmol) in THF at 0 °C. The solution was heated to 60 °C and stirred for 3 h, then cooled to room temperature. After evaporation of the solvent, the residue was purified by chromatograph. Yield: 76%. ^{1}H NMR (ppm, $CDCl_3$): 0.58 (br, 4H), 1.07–1.45 (m, 24H), 1.73–1.80 (m, 4H), 1.83–1.94 (m, 4H), 2.44 (s, 6H), 4.00 (t, 4H), 6.98 (d, J = 9 Hz, 4H), 7.31 (d, J = 8.7 Hz, 4H), 7.44–7.46 (m, 4H), 7.50–7.54 (m, 2H), 8.00 (d, J = 8.1 Hz, 4H), 8.03 (d, J = 9 Hz, 4H). Anal. Calcd for $C_{63}H_{68}Br_2N_4O_4$: C, 68.47; H, 6.20; N, 5.07. Found: C, 68.38; H, 6.28; N, 4.80.

M2

Yield: 82%. ^{1}H NMR (ppm, $CDCl_3$): 0.58 (br, 4H), 1.06–1.48 (m, 24H), 1.80–1.90 (m, 4H), 1.91–1.94 (m, 4H), 2.45 (s, 6H), 4.07 (t, 4H), 7.15 (s, 2H), 7.19 (d, J = 8.7 Hz, 2H), 7.33 (d, J = 8.4 Hz, 4H), 7.43–7.46 (m, 4H), 7.50–7.53 (m, 2H), 7.81 (d, J = 8.4 Hz, 2H), 7.83 (d, J = 8.7 Hz, 2H), 8.05 (d, J = 8.4 Hz, 4H), 8.12 (d, J = 8.7 Hz, 4H), 8.51 (s, 1H). Anal. Calcd for $C_{71}H_{72}Br_2N_4O_4$: C, 70.76; H, 6.02; N, 4.65. Found: C, 70.70; H, 6.18; N, 4.60.

M3

Yield: 73%. ^{1}H NMR (ppm, $CDCl_3$): 0.58 (br, 4H), 1.06–1.58 (m, 24H), 1.75–1.80 (m, 4H), 1.89–1.94 (m, 4H), 2.45 (s, 6H), 3.99 (t, 4H), 6.97 (d, J = 8.4 Hz, 4H), 7.33 (d, J = 8.4 Hz, 4H), 7.44-7.47 (m, 4H), 7.51–7.54 (m, 2H), 7.57 (d, J = 8.4 Hz, 4H), 7.70 (d, J = 8.4 Hz, 4H), 8.03 (d, J = 8.1 Hz, 4H), 8.16 (d, J = 8.1 Hz, 4H). Anal. Calcd for $C_{75}H_{76}Br_2N_4O_4$: C, 71.65; H, 6.09; N, 4.46. Found: C, 71.31; H, 6.27; N, 4.49.

M4

Yield: 89%. ^{1}H NMR (ppm, $CDCl_3$): 0.51 (br, 4H), 1.07–1.26 (m, 8H), 1.68–1.70 (m, 4H), 1.77–1.82 (m, 4H), 4.17 (t, 4H), 7.19 (t, 4H), 7.28–7.35 (m, 6H), 7.40–7.48 (m, 8H), 8.05 (d, J = 7.8 Hz, 4H). Anal. Calcd for $C_{49}H_{46}Br_2N_2$: C, 71.53; H, 5.64; N, 3.41. Found: C, 71.77; H, 5.98; N, 3.43.

Polymerization

The synthetic route of polymers is shown in Scheme 2. A general procedure of polymerization is proceeded through the Suzuki coupling reaction. For polymers P1–P3, a mixture of 2,7-bis(4,4,5,5-tetramethyl-1,3,2-dioxaborolan-2-yl)-9,9-dihexyllfluorene (1 equiv), dibromo compound (1 equiv), and tetrakis(triphenylphosphine) palladium (1.0 mol %) were added in a degassed mixture of toluene ([monomer] = 0.2M) and aqueous 2M potassium carbonate (3:2 in volume). The mixture was vigorously stirred at 87 °C for 72 h. After the mixture was cooled to room temperature, it was poured into 200 mL of methanol. A fibrous solid was obtained by filtration. The solid was washed sequentially with methanol, water, and methanol. A similar procedure is carried out for the synthesis of P4, and the feed ratio of 2,7-bis(4,4,5,5-tetramethyl-1,3,2-dioxaborolan-2-yl)-9,9-dioctylfluorene/M1/M4 is 2/1/1. The actual m/n ratio of the resulting polymer (P4) is about 1:1, which is calculated from proton NMR.

P1

Yield: 53%. ^{1}H NMR (ppm, $CDCl_3$): 0.77–1.38 (m, 50H), 1.70–1.76 (m, 4H), 2.11 (br, 8H), 2.42 (s, 6H), 3.96 (t, 4H), 6.95 (d, J = 8.7 Hz, 4H), 7.29 (d, J = 8.1 Hz, 4H), 7.68–7.85 (m, 12H), 7.98–8.04 (m, 8H). Anal. Calcd for $C_{88}H_{100}N_4O_4$: C, 82.72; H, 7.89; N, 4.38. Found: C, 82.72; H, 7.89; N, 4.05.

P2

Yield: 61%. ^{1}H NMR (ppm, $CDCl_3$): 0.77–1.41 (m, 50H), 1.75–1.80 (m, 4H), 2.12 (br, 8H), 2.42 (s, 6H), 4.00 (t, 4H), 7.09–7.21 (m, 4H), 7.30–7.35 (m, 4H), 7.68–7.85 (m, 16H), 8.02–8.15 (m, 6H), 8.48 (s, 2H). Anal. Calcd for $C_{96}H_{104}N_4O_4$: C, 83.68; H, 7.61; N, 4.07. Found: C, 82.93; H, 7.60; N, 3.82.

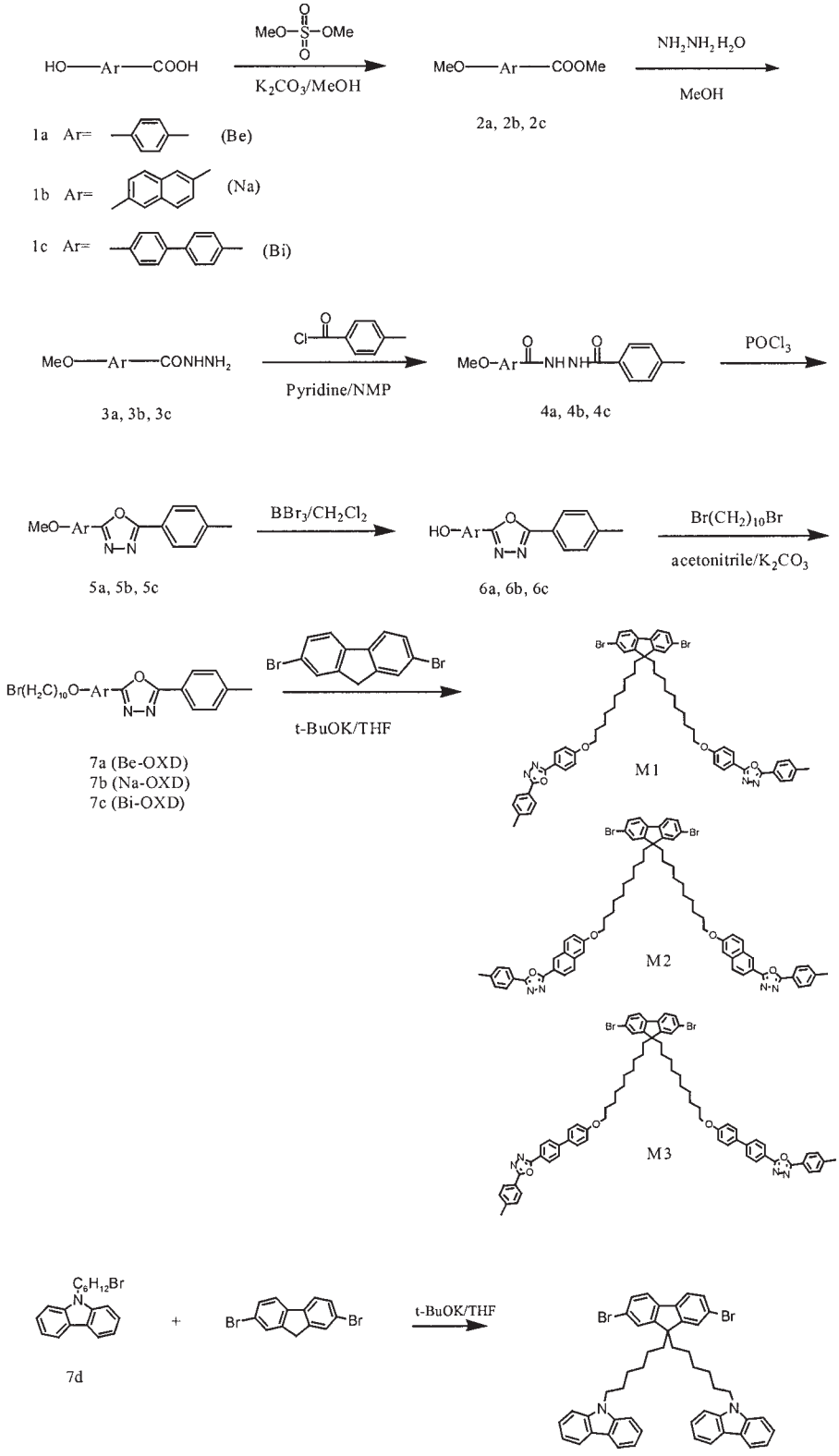

Scheme 1. Synthetic routes of monomers.

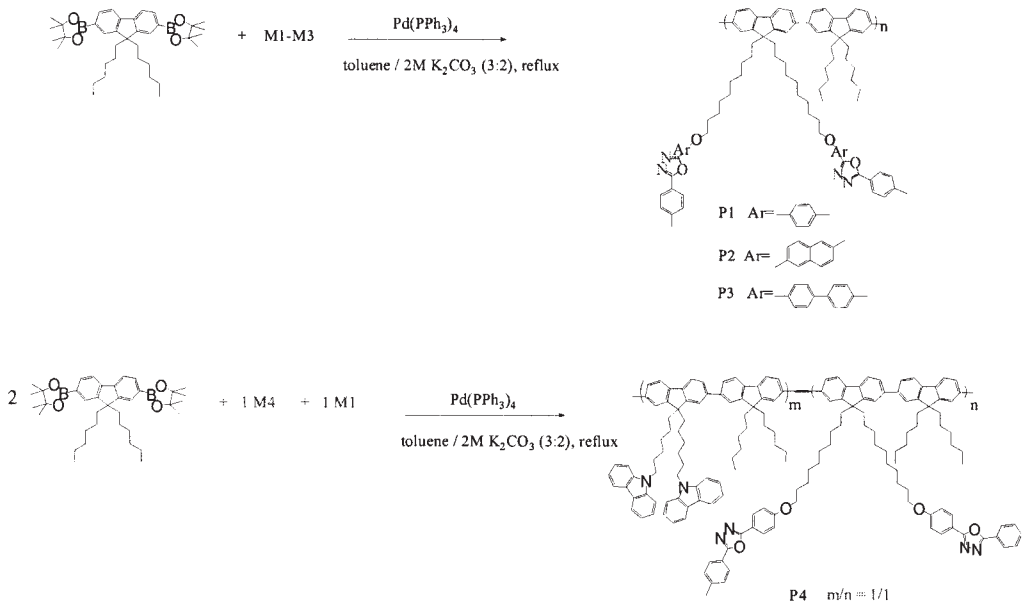

Scheme 2. Synthetic route of polymers.

P3

Yield: 79%. ^{1}H NMR (ppm, $CDCl_3$): 0.77–1.38 (m, 50H), 1.67–1.73 (m, 4H), 2.13 (br, 8H), 2.42 (s, 6H), 3.93 (t, 4H), 6.93 (d, J = 8.4 Hz, 4H), 7.30 (d, J = 7.8 Hz, 4H), 7.53–7.82 (m, 20H), 8.00 (d, J = 7.8 Hz, 4H), 8.12 (d, J = 8.4 Hz, 4H). Anal. Calcd for $C_{100}H_{108}N_4O_4$: C, 83.99; H, 7.61; N, 3.92. Found: C, 83.61; H, 7.61; N, 3.67.

P4

Yield: 82%. ^{1}H NMR (ppm, $CDCl_3$): 0.65–1.40 (m, 84H), 1.78 (br, 8H), 2.11 (br, 16H), 3.98 (t, 4H), 4.18 (br, 4H), 6.94 (d, J = 9 Hz, 4H), 7.15 (t, 4H), 7.25–7.36 (m, 12H), 7.60–7.88 (m, 24H), 7.96–8.05 (m, 12H).

RESULTS AND DISCUSSION

Synthesis and Characterization

Our previous study reveals that 2-(6-alkoxy-naphthalen-2-yl)-5-phenyl-1,3,4 oxadiazoles containing various substituents at the phenyl 4-position (*n*-NPO-X) exhibit stable mesogenic properties as shown in Structure 1,

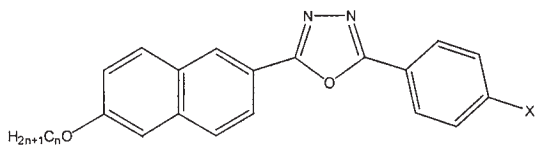

n-NPO-X

where n = 6, 8, and 10, and X = Me, OMe, F, Cl, CN, and NO_2[25], including the nematic and SmA phases.[25] These LC materials incorporated with strong polar electron-withdrawing terminal groups (F, Cl, CN, and NO_2) exhibit the SmA phase and tend to form a highly ordered smectic E (SmE) phase. Whereas, when electron-donating methyl and methoxy groups were served as terminal moieties, the mesophase of these LC materials do not show any SmE phase. Although the methoxy-substituted material (*n*-NPO-OMe) exhibits wider mesophasic temperature range than that of methyl-substituted materials (*n*-NPO-Me), choosing the methoxy group as a terminal group of the mesogenic pendant in this research will encounter a synthetic problem by converting a methoxy group into a hydroxy group (synthetic step 5 of Scheme 1). Therefore, the methyl group becomes our best choice of the terminal group. Besides, 10-NPO-Me possesses monotropic nematic and SmA phases along with the widest mesophasic temperature range (I 107 N 93 SmA 85 K) among these *n*-NPO-Me. Concluding the aforementioned views, we can formulate the optimal structure (Na-OXD, 7b) that possesses decyloxy side-chain spacers and methyl terminal groups as electron-transporting mesogenic pendants, which are attached to the PF backbones. Comparatively, we also introduce non-mesogenic pendants (Be-OXD, 7a, and carbazole, 7d) and mesogenic pendants (Bi-OXD, 7c, with wider mesophasic temperature range, i.e. K 134 SmA 187 N 195 I) to the PF backbones. In addi-

tion, polymers containing OXD pendants can provide large steric hindrance and reduce aggregation, which also have been reported.[10,31] To our best knowledge, the first series of PF copolymers containing PF backbones and electron-transporting mesogenic pendants are reported in this research.

The average molecular weights of these PF copolymers obtained by GPC are given in Table 1. The number-average-molecular weights (M_n) of polymers are between 10,200 and 55,700 g/mol, and the polydispersity indices (PDI) are between 1.8 and 2.6. The thermal stability of the polymers in nitrogen evaluated by thermogravimetric analysis (TGA) indicates that the degradation temperatures (T_d) of 5% weight loss in nitrogen are larger than 400 °C for all polymers (shown in Table 1). The mesomorphism characterized by polarizing optical microscopy (POM) and differential scanning calorimetry (DSC) thermograms are displayed in Figure 1. To avoid thermal decomposition, these polymers were heated to 280 °C, then subsequently cooled to −40 °C at a heating and cooling rate of 10 °C/min, whereas their melting temperatures were not observed even up to 280 °C. The DSC results show the glass transition temperatures of these polymers are between 60 and 101 °C (demonstrated in Table 1). All these polymers are found to display the nematic and SmA phases, and reveal isotropization temperatures above 340 °C (except P1) where thermal decomposition occurred.

Poly(9,9-dioctylfluorene) (PFO) and chiral PF containing 2S-methylbutyl side groups have been reported to exhibit mesomorphism but with a strong tendency to crystallize on both heating and cooling processes.[23] Herein, we introduce electron-transporting Be-OXD (7a) groups, which

Table 1. Molecular Weights and Thermal Properties of Polymers P1–P4

Polymer	Yield (%)	M_n	M_w/M_n	T_d[a] (°C)	T_g (°C)	T_c (°C)[b]
P1	53	10200	2.2	406	60	> 300
P2	61	27000	2.1	414	80	> 340
P3	79	55700	2.6	438	86	> 340
P4	82	45600	1.8	438	83	> 340

[a] Temperature of 5% weight loss measured by TGA in nitrogen.
[b] Temperature measured by polarizing optical microscopy (POM).

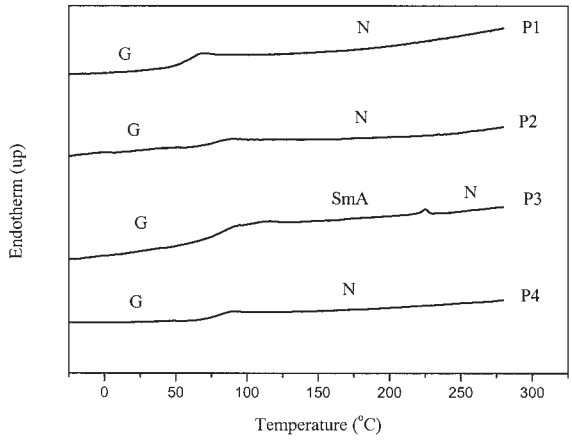

Figure 1. DSC thermograms of polymers during the second heating scan at 10 °C/min. Symbols: G, glass; N, nematic; K, crystalline.

do not exhibit mesogenic properties, to PF backbones to serve as pendants of the resulting polymer (P1). As revealed by DSC diagram (shown in Fig. 1), P1 is an amorphous polymer with T_g = 60 °C and shows a stable glass-forming nematic phase corroborated by polarizing optical microscopy. P2 contains Na-OXD (7b) pendants, which is a monotropic mesogenic material with nematic and SmA phases, shows T_g = 80 °C, and only exhibits a nematic phase without any SmA phase. On the other hand, P3 possesses Bi-OXD (7c) groups as pendants, and Bi-OXD has wider mesophasic temperature range (K 134 SmA 187 N 195 I) than that of Na-OXD. The resulting polymer displays nematic and SmA phases similar to their pendants with T_g = 86 °C. In comparison with P2, P3 shows two mesophases including the nematic and SmA phases. The divergence may result from the wide SmA temperature range (53 °C) of Bi-OXD pendants, which induces the resulting polymer to exhibit the SmA phase. In contrast to Bi-OXD, Na-OXD only has SmA temperature range of 8 °C and consequently cannot effectively induce P2 to generate the SmA phase. Comparing P1 and P2-P3, we can find that although Be-OXD (7a) does not exhibit a mesogenic property, the large steric groups can still suppress the tendency of crystallinity and enhance the mesophasic temperature range. On the hand, P4 (which is a random copolymer comprising carbazole and Be-OXD groups) is also an amorphous polymer with T_g = 83 °C, and exhibits a nematic phase without any propensity to crystallize on heating or cooling. From these results, we can draw two conclusions. First, the

Table 2. Absorption and PL Emission Spectral Data of Polymers in Chloroform Solutions and Thin Solid Films

Polymer	$\lambda_{abs,sol}$ (nm)	$\lambda_{abs,film}$ (nm)	Optical Band Gap (eV)	$\lambda_{PL,sol}$ (nm)	$\lambda_{PL,film}$ (nm)	Φ_{PL}[a]	Φ_{PL}[b]
P1	300, 388	302, 389	2.95	417	427	1.06	0.80[c]
P2	325, 389	334, 394	2.95	417	428	1.07	0.89[d]
P3	320, 391	321, 395	2.95	417	428	1.09	0.95[d]
P4	296, 392	299, 395	2.95	417	428	1.04	—

[a] Excited at 370 nm (the absorption region of polymer backbones).
[b] Excited at absorption regions of pendant groups.
[c] Excited at the maximum absorbance of pendant groups.
[d] Excited at the absorption intersection of Na-OXD and Bi-OXD pendant groups.

mesomorphism of these conjugated polymers are greatly affected by the nature of the pendants. Second, the mesophasic temperature range will be hugely promoted, compared with the mesophasic temperature range of PFO ($\sim$ 100 °C), as well as the tendency of spontaneous crystallization of PF can be suppressed by the introduction of the OXD pendant groups.

Optical Properties

The photophysical properties of the pendants (7a–7c) and polymers are summarized in Tables 2 and 3 and Figures 2–5 serially. It is noticed that all polymers exhibit two absorption bands (Fig. 2). The shorter absorption range originates from the absorption of the pendants; the longer wavelength peak in the region of 360–400 nm is attributed to the electron transition of the conjugated PF backbones. The optical band gaps of the polymers from the edge absorption of the polymer solutions are all equivalent (2.95 eV) regardless of various pendants; the value is exactly the same with the optical band gap of PFO reported by Janietz.[32] The identical band gaps illustrate that the different pendant groups do not appreciably change the excited state of the polymers, which implies similar distribution of effective conjugation lengths in the solution state of these polymers.

The PL emission spectra in dilute solutions as well as in thin films are shown in Figure 3, where these polymers exhibit stable and strong purple-blue emissions from the PF backbones. Emissions from the OXD pendants are not observed, even when polymers are excited at the absorption peaks of the pendants. This indicates that the existence of efficient energy transfer from the pendants to the polymer backbones has occurred. Thin films and dilute solutions show nearly identical absorption values and shapes, indicating an absence of ground-state aggregation in the solid state. However, thin films show a redshift ca. 10 nm in PL peaks in contrast to dilute solutions, which suggests that light emission from a more planar structure has occurred in the solid state. The PL quantum yields are

Table 3. Absorption and PL Emission Spectral Data of Pendants in Chloroform

Pendant Group	λ_{abs}[a] (nm)	$\lambda_{PL,sol}$[b] (nm)	Rel. Φ_{PL}
Be-OXD (7a)	300	354	1[c]
Na-OXD (7b)	323	374	1.59[d]
Bi-OXD (7c)	319	386	1.75[d]

[a] Wavelength of the maximum absorbance.
[b] Wavelength of the maximum emission.
[c] Excited at 300 nm and the PL quantum yield sets as 1.
[d] Excited at the absorption intersection of Na-OXD and Bi-OXD.

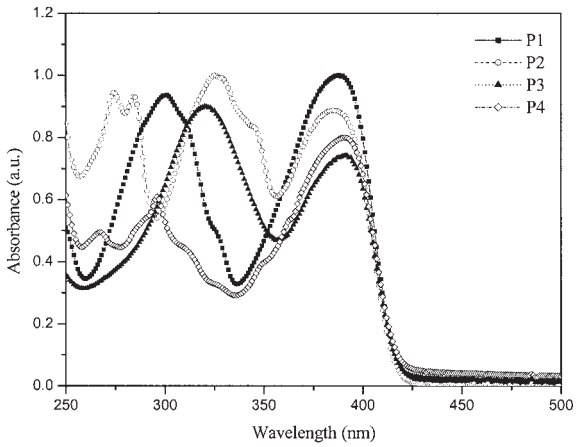

Figure 2. UV-visible spectra of polymer films.

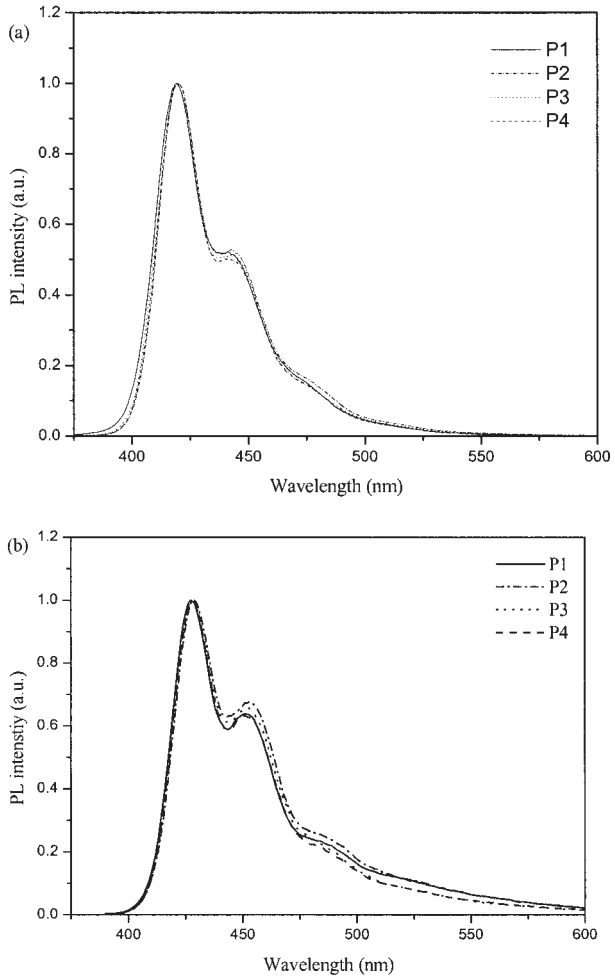

Figure 3. PL spectra of polymers: (a) in dilute chloroform solutions; (b) in films.

almost identical (Table 2) when these polymers are excited at the absorption region of the polymer backbone (370 nm). However, when these polymers are excited at the absorption region of pendants, the PL quantum yields (Table 2) will increase in the order of P1 < P2 < P3 according to the order of the quantum yield in each pendant (Table 3).

Owing to the glass-forming LC property of these polymers, they are suitable to generate polarized emissions. The anisotropic films are thermally annealed in the nematic temperature ranges on rubbing PI substrates for 30–60 min to align these polymers. As depicted in Figure 4, the shape of the annealed PL emissions is different from the thin film PL emissions, which indicates a more planar structure or aggregation formation in the annealed thin films. The PL dichroic ratios are 1.6 ~ 2.8 at 430 nm and 2.2 ~ 4.2 at 457 nm (Table 4), and these values

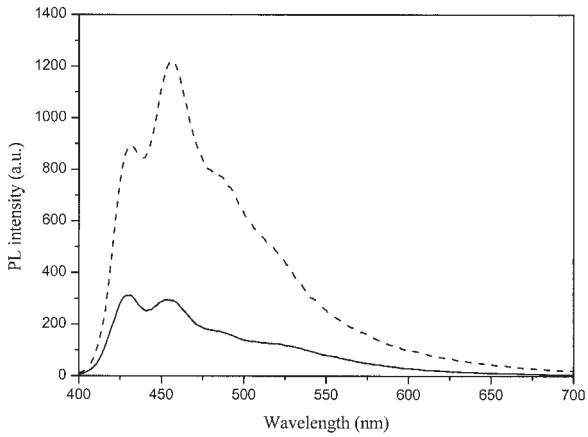

Figure 4. Polarized PL emission spectra of P3 annealed at the temperature range of the nematic phase. The spectra were measured as the polarized light parallel (dash line) and perpendicular (solid line) to the rubbing direction.

are relatively lower than that of PFO. It is noted that thermally treated films in LC state show remarkable anisotropic properties under polarizing optical microscope (POM). Unfortunately, the annealed films result in a weakly anisotropic light while the aligned films are cold from LC states. This result of fast relaxation in alignment may be due to a complex alignment morphology originated from the competition of the polymer backbone and the pendants under thermal alignment. Conversely, while P3 is annealed in the temperature range of the SmA phase, the PL spectrum of annealed film shows a red-shifted emission peak at ca. 544 nm (Fig. 5a). To identify the red-shifted emission peak that results from the aggregation (excimer formation) or the crystal packing (crystalline state) with different degrees of intermolecular interactions, P3 is sealed in an aligned LC cell with a thickness of 9 μm. The PL emission dichroic ratio is measured at 210 °C (which corresponds to the

Table 4. PL Emission Dichroic Ratios of Thermally Annealed Spin-Coated Films at Different Emission Peaks

Dichroic Ratio	P1	P2	P3	P4
R_{430}[a]	2.7	1.6	2.8	1.9
R_{457}[b]	3.8	2.4	4.2	2.9

[a] PL emission dichroic ratio measured at emission peak of 430 nm.
[b] PL emission dichroic ratio measured at emission peak of 457 nm.

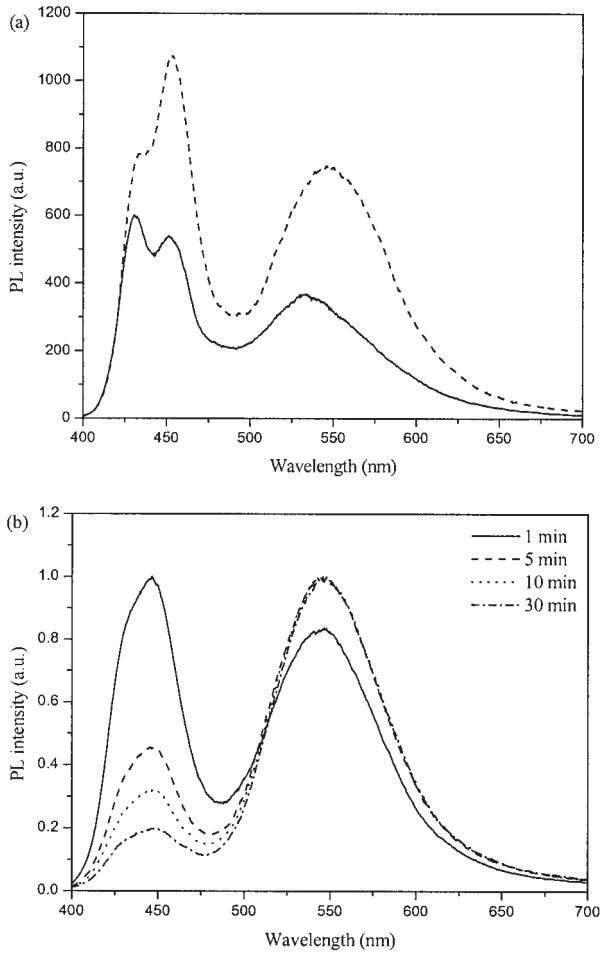

Figure 5. (a) Polarized PL emission spectra of P3 annealed at the temperature range of the SmA phase. The spectra were measured as the polarized light parallel (dash line) and perpendicular (solid line) to the rubbing direction. (b) Polarized PL emission spectra of P3 measured at 210 °C (the temperature range of the SmA phase) with different annealing time.

temperature range of the SmA phase) with different annealing time. As revealed in Figure 5b, the red-shifted peak becomes a dominated emission peak after 5 min thermal treatment and then becomes saturated after ca. 30 min treatment. From this result, we preferably assign the red-shifted emission band (ca. 544 nm) as an emission of the aggregation rather than the crystal packing. The dense packing of the smectic phase may be responsible for the formation of the aggregation. The data of PL dichroic ratios are summarized in Table 5; the emission dichroic ratios from polymer backbones and excimers are about 2.4 and 3.0, respectively, and these dichroic ratios are almost regardless of the annealing time.

Table 5. PL Emission Dichroic Ratios of P3 with Different Annealing Time at the Temperature Range of the SmA Phase

Dichroic Ratio	1 min	5 min	10 min	30 min
R_{446}[a]	2.2	2.6	2.4	2.3
R_{544}[b]	3.0	2.9	2.9	3.0

[a] PL emission dichroic ratio measured at emission peak of 446 nm.
[b] PL emission dichroic ratio measured at emission peak of 544 nm.

Electrochemical Properties

The redox behavior of polymer thin films were investigated by CV, and the potentials were estimated by the reference energy level of ferrocene (4.8 eV below the vacuum level) according to the following equation:[32] $E^{HOMO}/E^{LUMO} = [-(E^{onset} - 0.45) - 4.8]$ eV. The onset potentials were determined from the intersection of two tan-

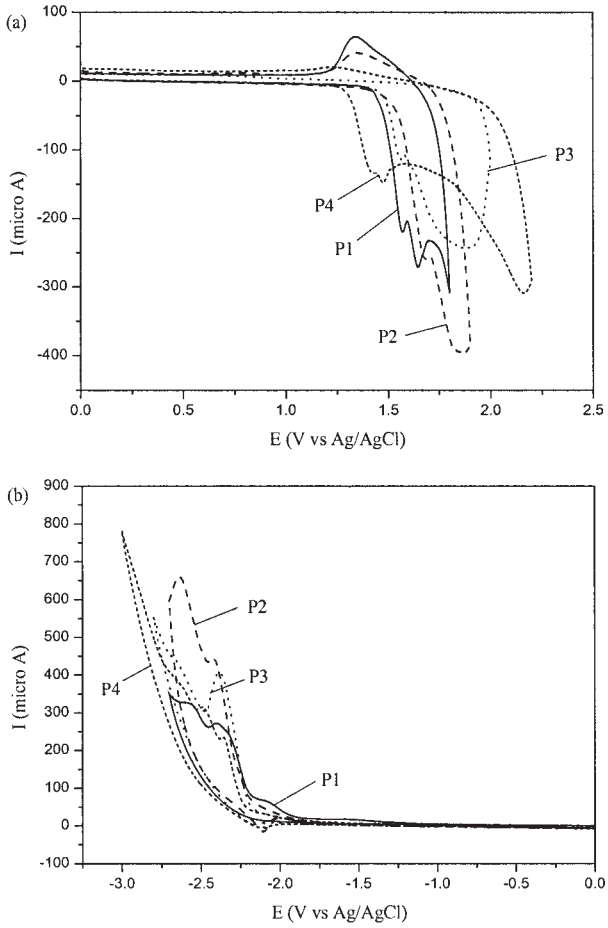

Figure 6. Cyclic voltammetry of polymers during (a) the oxidation process and (b) the reduction process.

Table 6. HOMO and LUMO Energies, and Electrochemical Properties of Polymers (P1–P4)

Polymer	$E^{red/onset}$ (V)	$E^{red/peak}$ (V)	$E^{ox/onset}$ (V)	$E^{ox/peak}$ (V)	E^{HOMO} (eV)	E^{LUMO} (eV)	Band Gap (eV)
P1	−1.91	−2.40, −2.59	1.46	1.57, 1.65	−5.81	−2.44	3.37
P2	−1.94	−2.42, −2.63	1.52	1.69, 1.87	−5.87	−2.41	3.46
P3	−1.86	−2.38, −2.67	1.47	1.56, 1.87	−5.82	−2.49	3.33
P4	−1.90	−2.36, −2.50	1.31	1.47, 2.16	−5.66	−2.45	3.21

gents drawn at the rising and background currents of the CV measurements. As shown in Figure 6, these polymers possess two anodic peaks, which can be attributed to the oxidation of both pendants and polymer backbones. The OXD substituted polymers (P1–P3) show the onset potentials of oxidation between 1.46 and 1.52 V (Table 6) in the anodic scans. The onset potentials are similar to that reported value of PFO (1.4 V),[32] and thus the onset potentials are due to the oxidation of the PF backbones. On the contrary, P4 has lower onset potentials of oxidation (ca. 1.31 V), and the lower value is attributed to the introduction of cabazole groups.[33] In the cathodic scans, the onset potentials of reduction are remarkably promoted from −2.28 V of PFO to ca −1.9 V of these polymers by introducing OXD groups. The electrochemical results indicate that the incorporation of the OXD and cabazole groups into PF as pendants will efficiently reduce the LUMO energy levels and promote the HOMO energy levels, thus reducing the energy barrier of charge injection from electrodes to emitters.

Electroluminescent (EL) Properties of PLED Devices

The EL data are summarized in Table 7. The current-voltage and luminescence-voltage characteristics are displayed in Figure 7. All these devices show similar turn-on voltages for current and light at ca. 5 V. These similar turn-on voltages for current and light illustrate that a matched balance of injection and transportation in charges is achieved. The device with P1 as an emitter has the highest luminance of 2104 cd/m^2 at 10 V (with a power efficiency of 1.13 cd/A at 100 mA/cm^2) among these OXD substituted polymers (P1–P3). The devices based on these polymers (P1–P3) demonstrate much higher maximum brightnesses than the device made of poly(9,9-dihexylfluorene),[34] which has a maximum brightness of 717 cd/m^2. In addition, the devices based on these polymers (P1–P3) also exhibit much better EL performance than the devices made of poly[9,9-bis(2′-ethylhexyl)fluorene-2,7-diyl] (PBEHF)[35] and poly(9,9-dioctylfluorene) (POF).[36] From these results, we can conclude that the incorporation of electron-transporting moieties (OXD) into hole-transporting PF backbones will improve the performance of the EL device. The device performance can be further improved by the incorporation of cabazole pendants into OXD-substituted PF (such as P4); a bright luminance of 2694 cd/m^2 at 11 V (with a power efficiency of 1.28 cd/A at 100 mA/cm^2) can be reached.

It was reported that EL emissions of PF suffer from the excimer formation on the current flow due to its liquid crystalline behavior,[37,38]

Table 7. PLED Devices[a] Performance Data

Polymer	λ_{max} (nm)	Voltage[b] (V)	Brightness[b] (cd/m^2)	Power Effiency[b] (cd/A)	Luminance Efficiency[b] (lm/W)	Max. Brightness (cd/m^2) (V)
P1	424	7.8	1134	1.13	0.46	2104 (10)
P2	422	7.2	802	0.80	0.35	1672 (11)
P3	424	7.6	1070	1.07	0.44	2036 (11)
P4	422	7.1	1276	1.28	0.56	2694 (11)

[a] Device structure: ITO/PEDOT:PSS/Polymer/Ca/Al.
[b] Measured at 100 mA/cm^2.

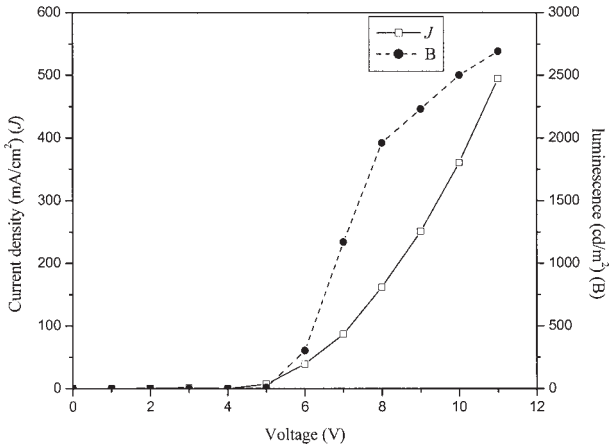

Figure 7. Current-voltage and luminescence-voltage characteristics of ITO/PEDOT:PSS/P4/Ca/Al device.

and result in an additional 100 nm bathochromic shifted emission at a lower energy band. As shown in Figure 8a, EL emission spectra of these polymers are almost the same at 8 V and exhibit stable EL emissions under forward biases. Figure 8b shows that the EL spectra of P3 are almost unchanged and without any low energy emission band as voltages increase from 6 V to 10 V. These EL spectra well match with the corresponding PL emission spectra of thin films, which indicates that the similar radiatively excited states are involved in both EL and PL processes. Consequently, we can successfully suppress the excimer formation in the PF backbones by introducing OXD groups with long flexible side chains, even though these polymers possess unfavorable liquid crystalline behavior for PLEDs devices.

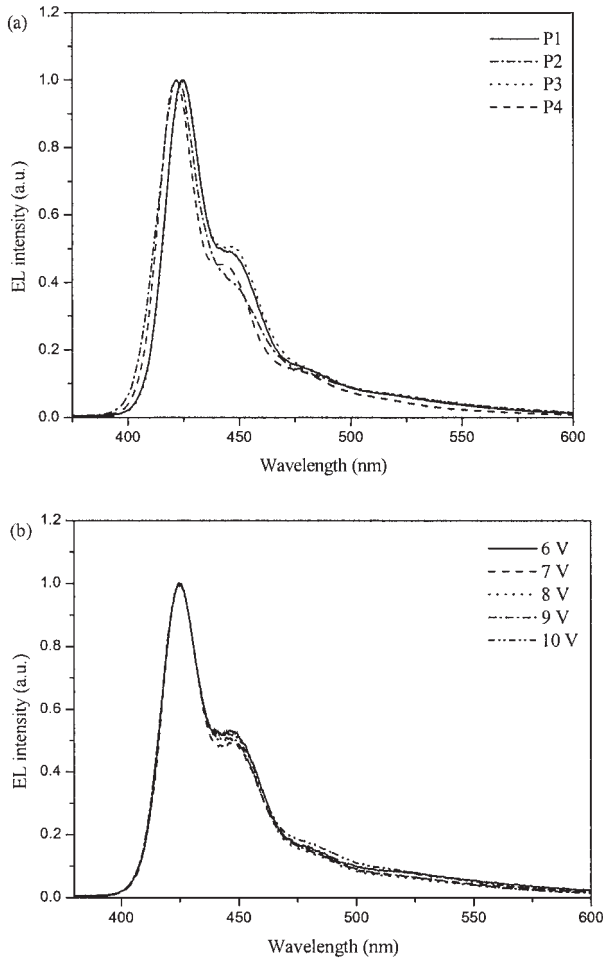

Figure 8. (a) Normalized EL spectra of ITO/PEDOT:PSS/Polymers/Ca/Al devices at 8 V. (b) Normalized EL spectra of ITO/PEDOT:PSS/P3/Ca/Al device at different voltages.

CONCLUSIONS

The thermal properties and mesomorphism of these glass-forming polymers are greatly affected by the nature of the pendants; these polymers exhibit stable mesogenic properties including the nematic and SmA phases. The incorporation of electron-transporting OXD pendants into PF backbones via long alkoxy spacers will effectively promote the mesophasic temperature range and depress the tendency of spontaneous crystallization of the PF backbones. For device performance, the introduction of charge-transporting pendants can not only tune the HOMO and LUMO energy levels but also suppress the formation of aggregation.

The authors gratefully acknowledge financial support from the National Science Council of Taiwan (ROC) through NSC 92-2113*M*-009-016.

REFERENCES AND NOTES

1. Redecker, M.; Bradley, D. D. C.; Inbasekaran, M.; Woo, E. P. Appl Phys Lett 1998, 73, 1565.
2. Grell, M.; Bradley, D. D. C.; Ungar, G.; Hill, J.; Whitehead, K. S. Macromolecules 1999, 32, 5810.
3. Klaerner, G.; Miller, R. D. Macromolecules 2007 1998, 31.
4. Chen, X.; Liao, J. L.; Liang, Y.; Ahmed, M. O.; Tseng, H. E.; Chen, S. A. J Am Chem Soc 2003, 125, 636.

5. Jenekhe, S. A.; Osaheni, J. A. Science 1994, 265, 765.
6. Samuel, I. D. W.; Rumbles, G.; Collison, C. J. Phys Rev B 1995, 52, R11573.
7. Ego, C.; Grimsdale, A. C.; Uckert, F.; Yu, G.; Srdanov, G.; Mullen, K. Adv Mater 2002, 14, 809.
8. Stetayesh, S.; Grimsdale, A. C.; Weil, T.; Enkelmann, V.; Mullen, K.; Meghdadi, F.; List, E.; J. W.; Leising, G. J Am Chem Soc 2001, 123, 946.
9. Marsitzky, D.; Vestberg, R.; Blainey, P.; Tang, B. T.; Hawker, C. J.; Carter, K. R. J Am Chem Soc 2001, 123, 6965.
10. Wu, F. I.; Reddy, S.; Shu, C. F.; Liu, M. S.; Jen, A. K. Y. Chem Mater 2003, 15, 269.
11. Shu, C. F.; Dodda, R.; Wu, F. I.; Liu, M. S.; Jen, A. K. Y. Macromolecules 2003, 36, 6698.
12. Scherf, U.; List, E. J. W. Adv Mater 2002, 14, 477.
13. Grel, M.; Bradley, D. D. C.; Inbasekaran, M.; Woo, E. P. Adv Mater 1997, 9, 798.
14. Hamaguchi, M.; Yoshino, K. Appl Phys Lett 1995, 67, 3381.
15. Geng, Y.; Chen, A. C. A.; Ou, J. J.; Chen, S. H. Chem Mater 2003, 15, 4352.
16. Whitehead, K. S.; Grell, M.; Bradley, D. D. C.; Jandke, M.; Strohriegl, P. Appl Phys Lett 2000, 76, 2946.
17. Banach, M. J.; Friend, R. H.; Sirringhaus, H. Macromolecules 2003, 36, 2838.
18. Grell, M.; Redecker, M.; Whitehead, K. S.; Bradley, D. D. C.; Inbasekaran, M.; Woo, E. P; Wu, W. Liq Cryst 1999, 26, 1403.
19. Miteva, T.; Meisel, A.; Knoll, W.; Nothofer, H. G.; Scherf, U.; Muller, D. C.; Meerholz, K.; Yasuda, A.; Neher, D. Adv Mater 2001, 13, 565.
20. Schartel, B.; Wachtendorf, V.; Grell, M; Bradley, D. D. C.; Hennecke, M. Phys Rev B 1999, 60, 277.
21. Sainova, D.; Zen, A.; Nothofer, H. G.; Asawapirom, U.; Scherf, U.; Hagen, R.; Bieringer, T.; Kostromine, S.; Neher, D. Adv Funct Mater 2002, 12, 49.
22. Culligan, S.W.; Geng, Y.; Chen, S. H.; Klubek, K.; Vaeth, K. M.; Tang, C. W. Adv Mater 2003, 15, 1176.
23. Geng, Y.; Trajkovska, A.; Katsis, D.; Ou, J. J.; Culligan, S. W.; Chen, S. H. J Am Chem Soc 2002, 124, 8337.
24. Geng, Y.; Culligan, S. W.; Trajkovska, A.; Wallace, J. U.; Chen, S. H. Chem Mater 2003, 15, 542.
25. Song, H. H.; Lin, H. C. Liq Cryst 2004, 31, 831.
26. Peng, Z.; Bao, Z.; Galvin, M. E. Chem Mater 1998, 10, 2086.
27. Ranger, M.; Rondeau, D.; Leclerc, M. Macromolecules 1997, 30, 7686.
28. Contoret, A. E. A.; Farrar, S. R.; O'Neill, M.; Nicholls, J. E; Richards, G. J.; Kelly, S. M.; Hall, A. W. Chem Mater 2002, 14, 1477.
29. Barry, J.; Bram, G.; Decodts, G.; Looupy, A.; Orange, C. Synthesis 1985, 1, 40.
30. Liu, S. P.; Chan, H. S. O.; Ng, S. C. J Polym Sci Part A: Polym Chem 2004, 42, 4792.
31. Sung, H. H.; Lin, H. C. Macromolecules 2004, 37, 7945.
32. Janietz, S.; Bradley, D. D. C.; Grell, M.; Giebeler, C.; Inbasekaran, M.; Woo, E. P. Appl Phys Lett 1998, 73, 2453.
33. Xia, C.; Advincula, R. C. Chem Mater 2001, 13, 1682.
34. Liu, M. S.; Jiang, X.; Herguth, P.; Jen, A. K. Y. Chem Mater 2001, 13, 3820.
35. Hwang, D. H.; Kim, S. K.; Park, M. J.; Lee, J. H.; Koo, B. W.; Kang, I. N.; Kim, S. H.; Zyung, T. Chem Mater 2004, 16, 1298.
36. Gong, X.; Iyer, P. K.; Moses, D.; Bazan G. C.; Heeger, A. J. Adv Funct Mater 2003, 13, 325.
37. Weinfurtner, K. H.; Fujikawa, H.; Tokito, S.; Taga, Y. Appl Phys Lett 2000, 76, 2502.
38. Bradley, D. D. C.; Grell, M.; Long, X.; Mellor, H.; Grice, A. Proc SPIE 1998, 3145, 254.